Analysis of boundary slip in a flow with an oscillating wall

Joseph John Thalakkottor[1,*] and Kamran Mohseni[1,2,†]

[1]*Department of Mechanical and Aerospace Engineering, University of Florida, Gainesville, Florida 32611, USA*
[2]*Department of Electrical and Computer Engineering, University of Florida, Gainesville, Florida 32611, USA*

Molecular dynamics (MD) simulation is used to study slip at the fluid-solid boundary in an unsteady flow based on the Stokes' second problem. An increase in slip is observed in comparison to the steady flow for shear rates below the critical shear rate of the corresponding steady flow. This increased slip is attributed to fluid inertial forces not represented in a steady flow. An unsteady mathematical model for slip is established, which estimates the increment in slip at the boundary. The model shows that slip is also dependent on acceleration in addition to the shear rate of fluid at the wall. By writing acceleration in terms of shear rate, it is shown that slip at the wall in unsteady flows is governed by the gradient of shear rate and shear rate of the fluid. Nondimensionalizing the model gives a time dependent yet universal curve, independent of wall-fluid properties, which can be used to find the slip boundary condition at the fluid-solid interface based on the information of shear rate, gradient of shear rate of the fluid, and the instant of time during the cycle. A governing nondimensional number, defined as the ratio of phase speed to speed of sound, is identified to help in explaining the mechanism responsible for the transition of slip boundary condition from finite to a perfect slip and determining when this would occur. Phase lag in fluid velocity relative to wall is observed. The lag increases with decreasing time period of wall oscillation and increasing wall hydrophobicity. The phenomenon of hysteresis is seen when looking into the variation of slip velocity as a function of wall velocity and slip velocity as a function of fluid shear rate. The cause for hysteresis is attributed to the unsteady inertial forces of the fluid. The rate of heat generated by viscous shear is compared for an unsteady Stokes' second problem and simple Couette flow and is shown to be higher for the unsteady flow.

I. INTRODUCTION

The no-slip boundary condition at the interface of a fluid and a solid wall has been the subject of many investigations for more than a century [1–3]. Navier [4] was the first to introduce the linear boundary condition, which was later also proposed by Maxwell [5], and it remains the standard characterization of slip even today. Slip at the boundary although prevalent, is negligibly small in most continuum and macroscale applications. Hence, the no-slip boundary condition is widely accepted and has been shown to give accurate results in such applications. However, in many micro- and/or nanoscale applications the first breakdown of continuum assumption often occurs at a solid boundary in the form of velocity slip.

As transport in ever smaller scales is considered, surface forces and effects start playing a more profound role on fluid transport than the bulk forces. Results from various computer simulations [6–15], which have been backed up by a number of laboratory experiments [16–23], show the presence of slip in fluids at the boundary. The advent of molecular dynamics simulations proved to be a considerable aid in understanding slip, as performing experiments at such scales is difficult. Most MD simulations have been focused on steady flows. MD simulations of a shear-driven steady flow by Thompson and Robbins [14] showed dependence of slip on wall-fluid properties such as density of the wall relative to fluid, the strength of liquid-solid coupling, and the thermal roughness

of the interface. They also observed layering of fluid normal to solid walls [14]. Thompson and Troian [15] performed MD simulation of the steady Couette flow. They observed that at small shear rates the boundary condition is consistent with the Navier model. However, as the shear rate is increased the Navier condition breaks down and the slip length increases rapidly with shear rate. They discovered that as the wall velocity is increased the slip at the wall is nonlinearly increased to infinity at a critical shear rate at which point the wall is no longer able to impart any further momentum to the fluid. They also went on to find a universal curve that gives the slip length for a specific shear rate irrespective of wall-fluid properties [15].

Boundary slip has been the subject of less investigation in unsteady flows. A few exceptions are in unsteady gas flows [24,25] and analytic solutions for continuum scale problems [26–29]. However, to the authors' knowledge, for liquids at microscales the research has been limited to steady flows. To this end, channel flows with oscillatory wall movement, the so-called Stokes' second problem, appears as a natural extension of steady Couette flows investigated by Thompson and Troian. Such a flow can be encountered in several microsystem applications, such as microaccelerometers, inertial sensors, and resonant filters [30]. The preliminary results of this work were presented at APS DFD, 2011 [31] and at the AIAA conference, June 2012 [32].

In this paper the effects of unsteady flow on slip in simple liquids at the solid interface are presented. The numerical experiments conducted indicate that slip velocity is also dependent on fluid acceleration, in addition to the shear rate of the fluid. Previous studies on unsteady flows in microchannels by Khaled and Vafai [24], and Matthews and Hill [25] have used the Navier slip model, while Bahukudumbi *et al.* [33]

*tjjoseph@ufl.edu
†mohseni@ufl.edu

used the Maxwell slip model for their analysis. Both Navier's and Maxwell's models suggest the dependence of slip only on shear rate. To confirm our hypothesis, Maxwell's theory for slip in rarefied gases [5] for a steady flow is extended to an unsteady case. Although the original derivation is inspired based on some characteristics of gases, we will verify here that an analogous formulation is also valid for liquid flows. The unsteady slip model developed shows the existence of an additional acceleration term. Using the momentum equation the acceleration term can be rewritten as gradient of shear rate, hence showing that slip is dependent on shear rate and its gradient. Scaling the model by wall velocity and characteristic length for Stokes' second problem, collapses the data to give a time dependent yet universal curve, independent of wall-fluid properties, which can be used to find the slip boundary condition at the fluid-solid interface. It is seen that at the limiting case when unsteady flow tends to steady flow the model reduces back to Navier and Maxwell's model. We also introduce a nondimensional number that helps in explaining the transition of slip boundary condition from finite slip to perfect slip and determining when this would arise. Furthermore, the occurrence of hysteresis in unsteady flows is shown. Hysteresis is observed when comparing slip velocity with shear rate and slip velocity with wall velocity. The rate of heat generated by viscous shear is compared for an unsteady Stokes' second problem and simple Couette flow and has been shown to be higher for the unsteady flow as a result of higher shear stress in the flow. Our MD simulations reaffirm the findings by Karniadakis [30] which were made for gases and the experiments done by Alsten and Granick [34] that mention the increased energy dissipation in oscillatory shear flows.

Details of numerical experiments and code validation are specified in Secs. II and III. In Sec. IV an unsteady slip model is derived. Nondimensionalization of the model is discussed in Sec. V. Results and conclusion are presented in Secs. VI and VII, respectively.

II. NUMERICAL SETUP

The molecular dynamics simulations presented in this paper are performed using the LAMMPS package [35]. The problem geometry used is similar to that of Stokes' second problem which is achieved by selecting the height of the fluid channel to be greater than the Stokes' penetration depth, as shown in Fig. 1. The penetration depth as determined from the analytical solution of the Stokes' problem is given by $\delta = 6.51\sqrt{\nu/\omega}$, where ν is the kinematic viscosity of the fluid and ω is the frequency of wall oscillation. The channel dimensions and number of wall and fluid atoms for different wall densities and various time periods are presented in Table I. The fluid's initial state is modeled as a face-centered cubic (fcc) structure with the x direction of the channel being aligned along the $[11\bar{2}]$ orientation of the face-centered cubic lattice. The wall comprises two layers of atoms oriented along the (111) plane of fcc lattice. The wall atoms are fixed to their lattice sites. The bottom wall is kept stationary, while the top wall is subjected to an oscillatory motion, defined by

$$x = A\sin(\omega t), \quad (1)$$
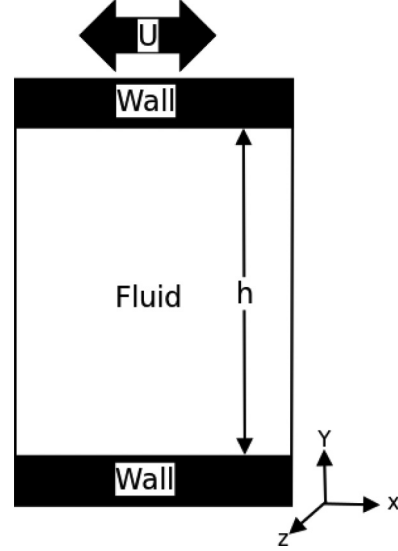
FIG. 1. Schematic of the problem geometry, where h is the height of the fluid channel and U is the wall velocity.

where A is the amplitude of wall oscillation. Periodic boundary conditions are imposed along the x and z directions.

The pairwise interaction of atoms separated by a distance r is modeled by the Lennard-Jones potential

$$V^{\text{LJ}} = 4\epsilon\left[\left(\frac{\sigma}{r}\right)^{12} - \left(\frac{\sigma}{r}\right)^{6}\right], \quad (2)$$

where ϵ and σ are the characteristic energy and length scales. The cutoff radius r_c is 2.2σ where the potential is zero for $r > r_c$.

The fluid is maintained in its equilibrium state having a number density $\rho = 0.81\sigma^{-3}$ and temperature $T = 1.1k_B/\epsilon$. The temperature is regulated by a thermostat which simulates the transfer of heat from the system to an external reservoir. A Langevin thermostat with a damping coefficient of $\Gamma = 1.0\tau^{-1}$, where $\tau = \sqrt{m\sigma^2/\epsilon}$, is used here. The damping term is only applied to the z direction to avoid biasing the flow. The equation of motion of the fluid atom of mass m along the z

TABLE I. Dimensions of the fluid domain and the number of fluid and wall atoms are enlisted for different values of time period. Time period T, wall number density ρ_w, length x, height y, and width z of the fluid channel, and the number of fluid N_f and wall N_w atoms are the variables mentioned. Here τ is the characteristic time of the Lennard-Jones potential and ρ is the fluid number density. The minor changes in the dimensions with change in wall density are done to make the problem geometry symmetric and periodic.

T/τ	ρ_w/ρ	x/σ	y/σ	z/σ	N_f	N_w
$\leqslant 120$	1	11.95	50	1204.14	595 000	23 100
$\leqslant 120$	4	12.14	50	1204.14	595 000	58 656
$\leqslant 400$	1	11.95	100	1204.14	1 190 000	23 100
$\leqslant 400$	4	12.14	100	1204.14	1 190 000	58 656
800	1	11.95	150	1204.14	1 785 000	23 100
800	4	12.14	150	1204.14	1 785 000	58 656

component is therefore given as follows:

$$m\ddot{z}_i = \sum_{j\neq i} \frac{\partial V_{ij}}{\partial z_i} - m\Gamma\dot{z}_i + \eta_i. \qquad (3)$$

Here $\sum_{j\neq i}$ denotes the sum over all interactions with i and η_i is a Gaussian distributed random force. The value of dynamic viscosity used for the calculations is $\mu = 2.0\epsilon\tau\sigma^{-3}$. The equations of motion were integrated using the Verlet algorithm [36,37] with a time step $\tau_c = 0.002\tau$.

The simulation is initially run for a time of $\sim 600\tau$ allowing the flow to equilibrate, after which, an ensemble average of required variables are taken in addition to spatial averaging. The spatial averaging is done along the length and width of the channel, with a bin height of 0.25σ.

III. VALIDATION OF SIMULATION

Before going ahead with our present experiment we validated our code by reproducing Thompson and Troian's results [15]. The problem consisted of a Couette flow geometry. Simulation was run for different cases having varying wall-fluid properties. For each case, slip length was computed for an increasing shear rate of fluid which in turn is governed by the wall velocity. The slip length is calculated from the linear Navier boundary condition $\Delta V = L_s\dot{\gamma}$, which can be simplified for Couette flow to $(U/\dot{\gamma} - h)/2$ [15], where ΔV is the slip velocity, L_s is the slip length, and $\dot{\gamma}$ is the fluid shear rate. The shear rate is computed as the slope of the velocity profile. The reproduced results of Thompson and Troian [15] are shown in Fig. 2. Considerable agreement was found with their results. The nonlinear dependence of slip length with shear rate is illustrated. Also we were able to duplicate the universal curve [15], which is a plot of slip length normalized by its limiting value L_S^o versus the shear rate which is normalized by the critical shear rate $\dot{\gamma}_c$. This primarily ends up collapsing the data onto one curve given by $L_s = L_s^o(1 - \dot{\gamma}/\dot{\gamma}_c)^{-1/2}$. The universal curve shows that for a given shear rate the nondimensionalized slip length is
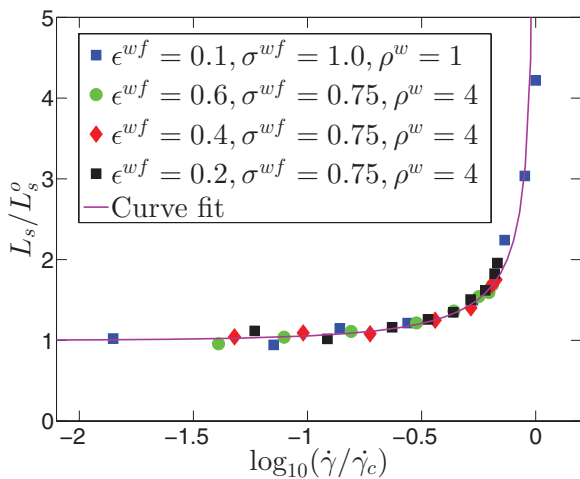
FIG. 2. (Color online) Universal curve describing the flow boundary condition. L_s and $\dot{\gamma}$ are scaled by L_s^0 and $\dot{\gamma}_c$, respectively. The curve fit is given by $L_s = L_S^0(1 - \dot{\gamma}/\dot{\gamma}_c)^{-1/2}$ in agreement with Thompson and Troian's results [15].

independent of the fluid wall properties of the problem being considered.

IV. UNSTEADY SLIP MODEL

The two widely used models, namely, Navier's and Maxwell's slip models, are in essence the same. Both show that the slip velocity at the fluid-solid interface is proportional to the shear rate of the fluid. Here we aim to capture the functionality associated with slip in fluids in unsteady flow by expanding Maxwell's theory. One of the reasons we resort to it is because of the lack of a widely accepted kinetic model for liquids. Even though Maxwell's model [5,38,39] was established for rarefied gases, we illustrate here that an analogous formulation can be made for slip in liquids. This is because the mechanism of slip at the wall is expected to have some similar features for both liquids and gases.

Maxwell's theory states that the reflection of fluid atoms after colliding with wall atoms can be categorized into two types: specular reflection and diffusive reflection, as shown in Fig. 3.

Diffusive reflection ($U_w^{f,\text{diff}}$). In this case the incident fluid atoms exhibit no slip and the velocity of the atom attained after collision is the same as that of the velocity of the wall during collision. This can be imagined as fluid atoms being adsorbed by the wall and then put back into the fluid in a random direction. Hence, the aggregate velocity of the atom after collision being equal to the velocity of wall atom at the instant of collision (relative velocity with wall being zero),

$$U_w^{f,\text{diff}}(t_c^+) = U^w(t_c). \qquad (4)$$

Here t_c is the instantaneous time of collision and U^w is the wall velocity.

Specular reflection ($U_w^{f,\text{spec}}$). The atoms undergo perfect slip and the velocity after collision is the same as that before collision:

$$U_w^{f,\text{spec}}(t_c^+) = U_w^f(t_c^-), \qquad (5)$$

where U_w^f is the fluid velocity at the wall. Furthermore, the velocity of the atom before collision with wall is deemed to have been obtained by collision with fluid atoms located at a distance equal to λ from the wall, this being the location of the first fluid layer and τ_c the time it takes for the fluid atom to travel this distance. Here we make an assumption that during the motion of the fluid atom in reference it is subjected to a net zero force during its journey from the first fluid layer to
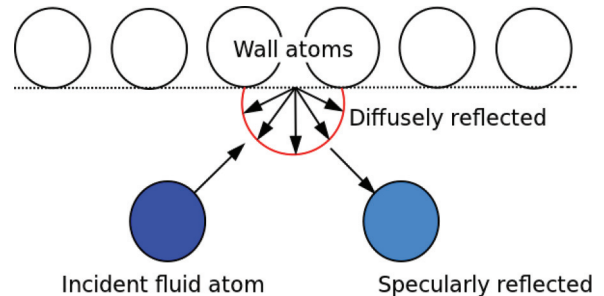
FIG. 3. (Color online) Schematic of diffusively and specularly reflected fluid atom.

the wall. Thereby, it has a constant velocity

$$U_w^f(t_c^-) = U_\lambda^f(t_c - \tau_c). \tag{6}$$

Performing a Taylor series expansion in space at the wall the velocity at a distance λ from it can be written as

$$U_\lambda^f(t_c - \tau_c) = U_w^f(t_c - \tau_c) - \lambda \frac{dU^f(t_c - \tau_c)}{dy}\bigg|_w. \tag{7}$$

Discretizing in time and ignoring all second and higher order terms we obtain

$$\begin{aligned} U_w^f(t_c^-) &= U_\lambda^f(t_c - \tau_c) \\ &= U_w^f(t_c) - \tau_c \frac{dU_w^f(t_c)}{dt} - \lambda \frac{dU^f(t_c)}{dy}\bigg|_w. \end{aligned} \tag{8}$$

Now, the average velocity after collision $U_w^f(t_c^+)$ is given by

$$U_w^f(t_c^+) = \sigma_d U_w^{f,\text{diff}}(t_c^+) + (1 - \sigma_d) U_w^{f,\text{spec}}(t_c^+), \tag{9}$$

where σ_d is called the tangential momentum accommodation coefficient (TMAC), which gives the fraction of atoms undergoing diffusive reflection. Substituting from Eqs. (4) and (5) in the above equation we obtain

$$U_w^f(t_c^+) = \sigma_d U^w(t_c) + (1 - \sigma_d) U_w^f(t_c^-). \tag{10}$$

The net instantaneous fluid velocity at the wall is given as the mean of the velocity before and after collision

$$U_w^f(t_c) = \frac{U_w^f(t_c^+) + U_w^f(t_c^-)}{2}. \tag{11}$$

By substituting $U_w^f(t_c^+)$ from (10), one obtains

$$2U_w^f(t_c) = \sigma_d U^w(t_c) + (2 - \sigma_d) U_w^f(t_c^-). \tag{12}$$

Now $U_w^f(t_c^-)$ could be replaced from Eq. (8) to give

$$\begin{aligned} 2U_w^f(t_c) = &\; \sigma_d U^w(t_c) + 2U_w^f(t_c) - \sigma_d U_w^f(t_c) \\ &+ (2 - \sigma_d)\left[-\tau_c \frac{dU_w^f(t_c)}{dt} - \lambda \frac{dU^f(t_c)}{dy}\bigg|_w \right]. \end{aligned} \tag{13}$$

Rearranging this equation results in

$$U^w(t_c) - U_w^f(t_c) = \frac{(2 - \sigma_d)}{\sigma_d}\left[\tau_c \frac{dU_w^f(t_c)}{dt} + \lambda \frac{dU^f(t_c)}{dy}\bigg|_w \right]. \tag{14}$$

Slip velocity is given as

$$U_s = U^w - U_w^f. \tag{15}$$

Using the definition of slip velocity Eq. (14) can be written as

$$U_s(t_c) = \frac{(2 - \sigma_d)}{\sigma_d}\left[\tau_c \frac{dU_w^f(t_c)}{dt} + \lambda \frac{dU^f(t_c)}{dy}\bigg|_w \right]. \tag{16}$$

Finally writing dU/dy in terms of shear rate $\dot\gamma$ we get

$$U_s(t_c) = \frac{(2 - \sigma_d)}{\sigma_d}\left[\tau_c \frac{dU_w^f(t_c)}{dt} + \lambda \dot\gamma\bigg|_w \right]. \tag{17}$$

Hence, we see that slip velocity has an additional dependence on the fluid acceleration at the wall in the case of unsteady flows.

The simplified Navier-Stokes equation is used in order to rewrite the acceleration term in the above expression in terms of shear rate. Writing down the two-dimensional momentum equation in x, with no external force or pressure gradient:

$$\frac{\partial u}{\partial t} + u\frac{\partial u}{\partial x} + v\frac{\partial u}{\partial y} = \nu\left(\frac{\partial^2 u}{\partial x^2} + \frac{\partial^2 u}{\partial y^2} \right). \tag{18}$$

In addition since the velocity of fluid in the x direction is uniform, the rate of change of velocity along the x direction goes to zero. Hence the Navier-Stokes equation reduces to

$$\frac{\partial u}{\partial t} = \nu\left(\frac{\partial^2 u}{\partial y^2} \right). \tag{19}$$

Now considering that $\dot\gamma = \frac{\partial U_w^f}{\partial y}$ one can rewrite the above equation as

$$\frac{\partial U_w^f}{\partial t} = \nu\frac{\partial}{\partial y}\left(\frac{\partial U_w^f}{\partial y} \right) = \nu\left(\frac{\partial \dot\gamma}{\partial y} \right). \tag{20}$$

Substituting this in the equation for slip velocity, Eq. (17), results in

$$U_s(t_c) = \frac{(2 - \sigma_d)}{\sigma_d}\left[\tau_c \nu\left(\frac{\partial \dot\gamma}{\partial y} \right) + \lambda \dot\gamma \right]_w. \tag{21}$$

For steady flow, slip velocity is seen to be proportional to the shear rate of the fluid as hypothesized by Navier and Maxwell. But here, we show that for an unsteady problem we have an additional contribution from the gradient of shear rate. Hence it is seen that the slip velocity for an unsteady case is proportional to the linear sum of shear rate and gradient of shear rate of the fluid at the wall.

In the limiting case when the flow approaches steady state and the acceleration goes to zero the unsteady slip model reduces back to that given by Maxwell:

$$U_s = \left(\frac{2 - \sigma_d}{\sigma_d} \right) \lambda \dot\gamma. \tag{22}$$

Comparing this to Navier's slip boundary condition

$$U_s = L_s\, \dot\gamma|_w, \tag{23}$$

one can write the slip length, $L_s = \frac{(2 - \sigma_d)}{\sigma_d}\lambda$. A σ_d value of one can be compared to a no-slip boundary condition in fluids where there is no relative velocity between the wall and fluid, while σ_d equal to zero corresponds to a boundary condition exhibiting perfect slip.

V. NONDIMENSIONALIZING THE UNSTEADY SLIP MODEL

Nondimensionalization of the slip model is performed with an attempt to simplify and parametrize the equation. It is also aimed at identifying a nondimensional parameter that could characterize unsteady slip. The unsteady slip model established in the previous section is scaled by the wall velocity U_w and the length scale associated with Stokes' second problem, $\sqrt{2\nu/\omega}$. Nondimensionalizing using this velocity

and length scale, one obtains

$$U_s^* = \left(\frac{2-\sigma_d}{\sigma_d}\right)\left[(\tau_c\nu)\frac{1}{\frac{2\nu}{\omega}}\left(\frac{\partial^2 U^{f*}}{\partial y^{*2}}\right) + \frac{\lambda}{\sqrt{\frac{2\nu}{\omega}}}\frac{\partial U^{f*}}{\partial y^*}\right]_w, \tag{24}$$

where $(\cdot)^*$ represents nondimensional quantities. Notice that, $\tau_c = \frac{\lambda}{\bar{c}}$, where $\bar{c}$ is the speed of sound in the fluid at a given temperature. Therefore

$$U_s^* = \left(\frac{2-\sigma_d}{\sigma_d}\right)\lambda^*\left[C_{nd}\frac{\partial^2 U^{f*}}{\partial y^{*2}} + \frac{\partial U^{f*}}{\partial y^*}\right]_w. \tag{25}$$

This could also be written as

$$U_s^* = L_s^*\left[C_{nd}\frac{\partial^2 U^{f*}}{\partial y^{*2}} + \frac{\partial U^{f*}}{\partial y^*}\right]_w, \tag{26}$$

which is the same as

$$U_s^* = L_s^*\left[C_{nd}\frac{\partial \dot{\gamma}^*}{\partial y^*} + \dot{\gamma}^*\right]_w, \tag{27}$$

where $L_s^* = (\frac{2-\sigma_d}{\sigma_d})\lambda^*$ and $C_{nd} = \frac{\sqrt{2\nu\omega}}{2\bar{c}}$ is the nondimensional parameter that controls the unsteady term based on the type of flow. As the fluid being used is liquid argon, slip length cannot be calculated from σ_d and λ directly, and hence Eq. (26) must be used. One can see that for a limiting case of $\omega = 0$, which corresponds to a steady flow problem, the equation reduces back to Maxwell's slip equation.

VI. RESULTS

The primary information that is extracted from the simulations is the fluid velocity. The following steps are taken before the data from the simulations is used for any analysis. First, a reference plane is defined at a distance of $0.5\sigma^{wf}$ away from the wall lattice site. This is the location at which the fluid variables at the wall are computed. Secondly, in order to obtain a well resolved velocity profile the Levenberg-Marquardt method [40,41] is used to fit the analytical solution of the Stokes' second problem to the data. This is done so as to limit the noise resulting from taking the derivatives of the velocity profile. Different cases of wall-fluid properties considered are listed in Table II.

Thompson and Troian [15] observed that the slip length for fluid shear rates much lower than the critical shear rate is constant. But for shear rates in the vicinity of the critical value it becomes highly nonlinear [15]. As we are here considering an unsteady problem the various fluid and wall variables are time varying, and so is the slip length if the shear rate is in the

TABLE II. Four different cases with varying wall-fluid properties were considered. ϵ^{wf} and σ^{wf} are the Lennard-Jones parameters for fluid-wall interaction.

Case	ϵ^{wf}/ϵ	σ^{wf}/σ	ρ_w/ρ
1	0.6	1.0	1
2	0.1	1.0	1
3	0.4	0.75	4
4	0.2	0.75	4

vicinity of its critical value. The details of how the slip length is calculated are described in the following section.

A. Verification of slip model

Several numerical simulations were conducted in order to verify the unsteady slip model established in the previous section. As the first test case the variation of slip length with time period while having a fixed wall amplitude is considered. This is presented for two different cases of wall-fluid properties in Fig. 4(a). These two cases correspond to cases 1 and 2 of Thompson and Troian [15] with the difference being that instead of a steady problem an unsteady problem is considered here. The slip length corresponding to each run can be calculated by fitting the data using the Levenberg-Marquardt method [40,41] and the slip model given in Eq. (26). In these plots we assume that the slip length is constant over a given
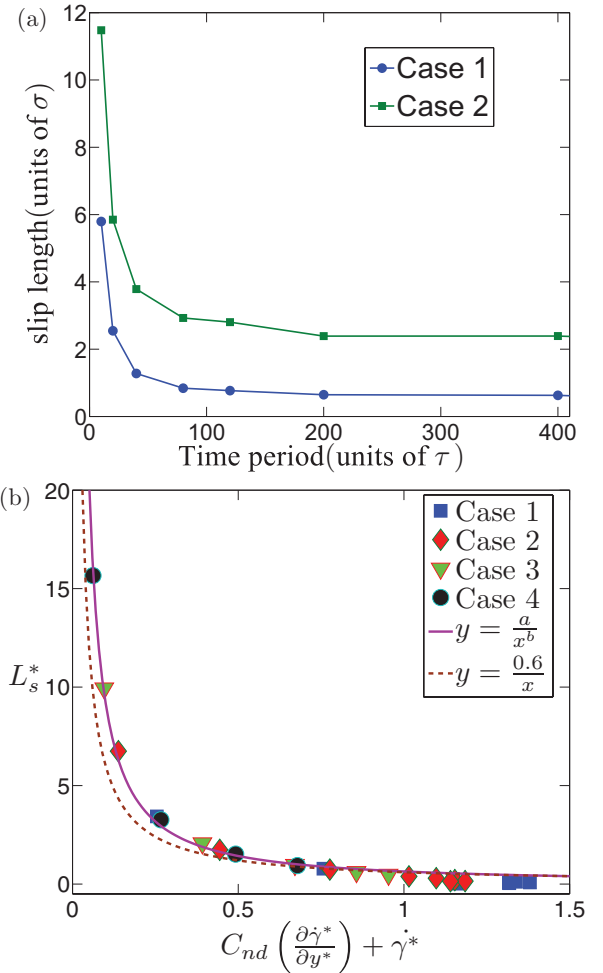
FIG. 4. (Color online) (a) Slip length versus time period. As the time period of the unsteady problem tends to a corresponding steady problem the steady state value of slip length is recovered. (b) Nondimensional slip length versus sum of the nondimensional shear rate and the product of nondimensional number C_{nd} and the gradient of shear rate. Here $y = L_s^*$ and $x = C_{nd}(\frac{\partial \dot{\gamma}^*}{\partial y^*}) + \dot{\gamma}^*$. The curve fitting parameters are computed to be $a = 0.64$, $b = 1.16$. It is seen that all the data for various cases considered collapse onto a single curve given by the fit for an instant of time.

cycle. This approach provides a single average value of slip length for each run. For runs with high time periods the maximum shear rate is below its critical value. It is shown by Thompson and Troian that for values below the critical shear rate the slip length is constant. Hence, we obtain quantitatively consistent results for high time periods, while for low time periods the average value helps in capturing the trend.

In Fig. 4(a) it is seen that the slip length approaches infinity as the wall oscillation frequency tends to infinity. This implies that the wall is oscillating at such a high frequency that no information can be passed on by the wall atoms to the underlying fluid atoms, thereby giving a perfect slip. As we increase the time period we observe that the slip length decreases and approaches an asymptotic finite value which corresponds to those shown by Thompson and Troian in the steady state Couette flow problem [15].

As a second test case the nondimensionalized slip length L_s^*, also mentioned as y, is plotted against x which is given as $[C_{nd}(\frac{\partial \dot{\gamma}^*}{\partial y^*}) + \dot{\gamma}^*]_w$, where x is a sum of the parameters that influence unsteady slip as seen in Fig. 4(b). In this plot the data considered correspond to an instant of time of maximum slip velocity in the cycle. The instantaneous value of slip length can be calculated from Eq. (26). The data for different cases of wall-fluid properties and different wall velocities collapse onto a single curve of the form $y = a/x^b$. In Fig. 4(b) it is shown that the curve can be described by the coefficients $a = 0.6$ and $b = 1.0$, given by the dashed line. The exact fitting coefficients to our experimental data were calculated to be $a = 0.64$ and $b = 1.16$, given by the solid line which fairly matches the dashed line. Hence, it is seen here that, similar to Thompson and Troian, proper scaling leads to a time dependent but universal curve (independent of the wall-fluid properties). This verifies the scaling parameters used for nondimensionalizing the slip model. The variation of nondimensional slip length is covered in more detail in Sec. VI E.

B. Relevance of nondimensional number

In the nondimensional number C_{nd}, $\sqrt{2\nu\omega}$ is the phase velocity of the propagating velocity profile in the y direction, whereas $\bar{c}$ is the speed of sound through the medium. The ratio can be physically seen as the ratio of propagation of momentum through the medium to the speed of propagation of sound through the medium. The maximum speed at which momentum can be transferred through a medium is at the speed of sound. Hence, when the phase speed is of the order of the speed of sound for the medium, the fluid will exhibit perfect slip as the wall would not be able to transfer momentum on to the fluid. The number can be used to determine when the boundary condition would change to perfect slip from a finite or no-slip condition.

C. Effects of acceleration on slip

In order to analyze the effect of acceleration on slip a wall-fluid property is chosen which is shown to exhibit no slip at the fluid-solid interface for steady flow by Thompson and Troian [15]. This corresponds to case 1 in Table II. Wall oscillation having an amplitude of 10σ and time period of 40τ is chosen such that the shear rate is considerably below its critical value.
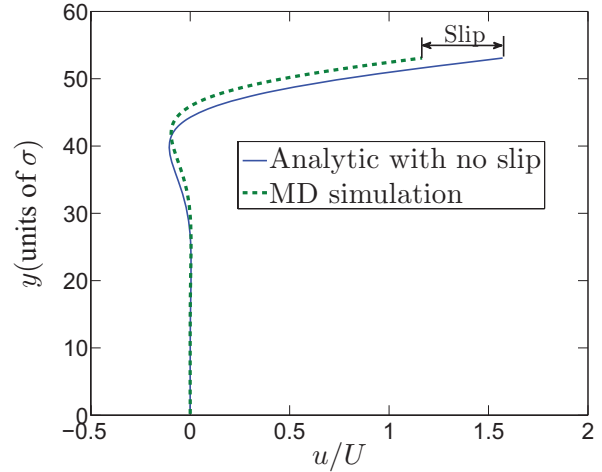
FIG. 5. (Color online) Velocity profile obtained from simulation with Stokes' analytical solution for the no-slip boundary condition is compared. The profile is for case 1 of wall-fluid properties and for an instant of time equal to the time period of wall oscillation. A distinct presence of slip at the wall is seen.

In Fig. 5, comparison of the velocity profile obtained from simulation is made with Stokes' analytical solution with the no-slip boundary condition. This is done for an instantaneous time $t = 40\tau$ for which distinct slip at the wall is observed.

1. Phase lag of fluid velocity due to wall acceleration

The presence of fluid slip at the wall indicates the existence of a lag of fluid velocity with respect to the wall. This is investigated by comparing fluid velocity for varying time periods of wall oscillation with the wall velocity as shown in Fig. 6. This is done to see the effects of acceleration on the fluid velocity. The comparison is made for case 1 of wall-fluid
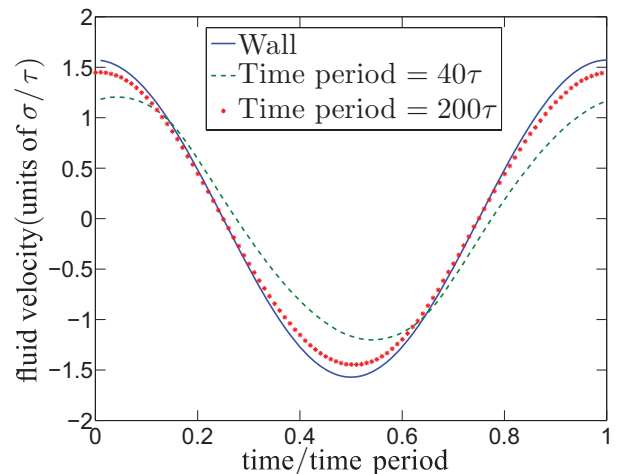
FIG. 6. (Color online) Comparison of wall velocity and fluid velocities at time periods 40τ and 200τ for a cycle of wall oscillation having wall-fluid properties corresponding to case 1. Amplitudes of 10σ and 50σ corresponding to the time periods of 40τ and 200τ are chosen in order to achieve the same amplitude of wall velocity in both cases. An increase in wall-fluid phase lag and a decrease in the amplitude of fluid velocity adjacent to the wall are observed by decreasing time period.
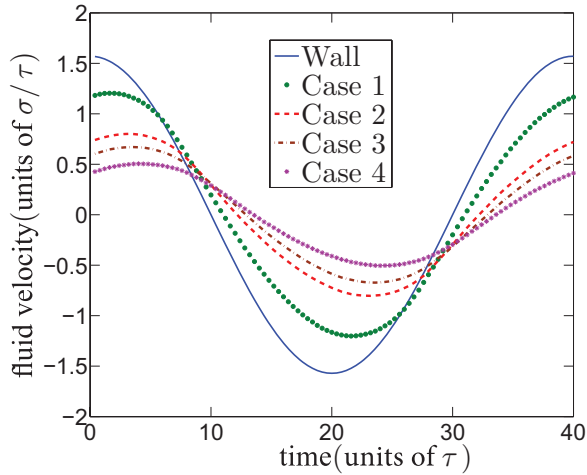
FIG. 7. (Color online) Velocities of wall and adjacent fluid in one wall oscillation cycle. The wall oscillation has an amplitude of 10σ and time period 40τ. An increase in wall-fluid phase lag and a decrease in the amplitude of fluid adjacent to the wall are observed by increasing the wall-fluid hydrophobicity.

FIG. 8. (Color online) Variation of fluid density along the height of fluid channel. Layering of fluid is observed close to the wall. The red dashed line marks the reference plane $0.5\sigma^{wf}$ away from the wall lattice site. The plot corresponds to case 1 with an amplitudes of 10σ and 40τ. As the layering is symmetric about the x-z plane only the top half is shown. The ordering is prevalent up to a distance of 5–6σ from the reference plane with decreasing amplitude beyond which the bulk density of the fluid is obtained.

properties. The amplitude of wall oscillation is calculated such that the amplitude of wall velocity remains constant. It is seen that the phase lag reduces and the amplitude of fluid velocity increases with increasing time period relative to the wall. An increase in time period results in a decrease in fluid inertia. Hence, it can be said that as we approach a steady state, by increasing time period, we recover the no-slip boundary condition for case 1, leading to the conclusion that inertia affects the slip of fluid at the wall, thereby confirming the general slip model derived in the previous section.

2. Phase lag of fluid velocity due to wall hydrophobicity

The variation of fluid velocity with time for different cases mentioned in Table II is shown in Fig. 7. This is done for a fixed time period of 40τ and wall amplitude of 10σ, the purpose being to see how the fluid velocity behaves with varying hydrophobicity. The fluid velocities lag with respect to the wall velocity. There is an increase in phase lag with increasing hydrophobicity. Also, a reduction in the amplitude of the fluid velocity is noticed. The phase lag and amplitude reduction are a result of the increase in slip. Matthews and Hill [25] in their analytical solution using the Navier slip model also see phase lag. Tang *et al.* [29] also observed similar phase lag of fluid velocity for different Stokes numbers and TMAC in their lattice Boltzmann simulation of oscillatory gas flows.

D. An explanation for the occurrence of slip

In this section a possible explanation for the occurrence of slip at the wall and increase in slip seen in unsteady flows as compared to steady flows is given. Increase in hydrophobicity leads to an increase in slip at the wall, which has been observed by several researchers for the steady case [6–15]. Strictly speaking, the no-slip boundary condition is only valid if the flow adjacent to a solid surface is in thermodynamic equilibrium [25,26]. For fluid flow in small-scale systems, the collision frequency is not high enough

to ensure thermodynamic equilibrium, thus a certain degree of tangential velocity slip must be allowed [25]. Also, these collisions should occur during a time interval smaller than that of the smallest time scale for flow changes. Harris and Rice calculated the relaxation time for liquid argon at 90 K as 0.5τ, while for gaseous argon at 300 K to be of the order of 100τ [42]. The relaxation time required for bulk liquid argon is small in comparison to the time scale of molecular collisions. However, as shown in Fig. 8, fluid layering is observed close to the wall. This leads to the reduction of liquid density and hence reduces the number of fluid atoms interacting and undergoing momentum transfer with the wall thereby increasing the required relaxation time [29]. Its also been shown by Granick that the relaxation time is prolonged for confined liquids [43]. Therefore, the fluid atoms adjacent to the wall do not have sufficient time to equilibrate and the transfer of momentum from the wall is only partial, therefore resulting in slip.

E. Boundary condition for an unsteady flow

One of the main aims of the studies pertaining to slip length is to find the boundary condition at the wall. As mentioned in Sec. VI A, the instantaneous value of the nondimensional slip length when plotted against the sum of shear rate and its gradient collapse onto a single curve, thereby providing a solution independent of wall-fluid properties similar to Thompson and Troian's result, the difference being that in the unsteady case there is a separate curve for a given instant in a cycle, as shown in Fig. 9. Here $t = 0$ corresponds to the maximum slip velocity during a cycle in a run. This is done in order to remove the phase shifts between different runs. It is observed that the data at various instants can be described by a curve of the form $y = a/x^b$. With the knowledge of shear rate, its gradient, and the instant in the cycle we can
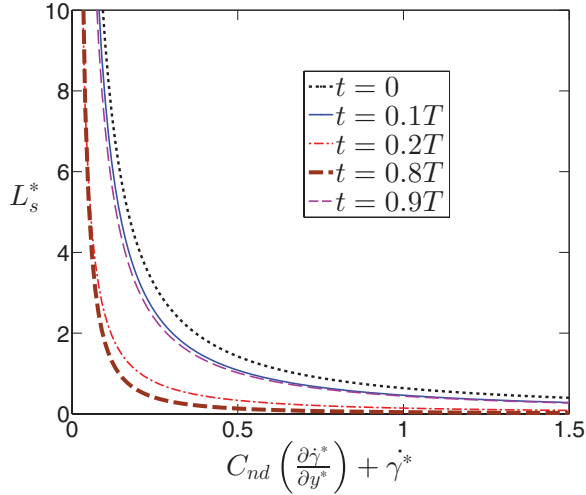
FIG. 9. (Color online) Data for different cases collapse onto a single curve defined by $y = \frac{a}{x^b}$, where $y = L_s^*$ and $x = C_{nd}(\frac{\partial \dot{\gamma}^*}{\partial y^*}) + \dot{\gamma}^*$ for a given instant in the cycle. Here the curves from the first quarter and fourth quarter in the cycle are presented. The other two quarters are symmetric to these. The fitting coefficients are mentioned in Table III.

determine the slip length. This helps in eliminating the need to perform extensive molecular dynamics simulations which are computationally expensive. On closely observing the fitted coefficients listed in Table III we see that the coefficients in the first quarter of the wall oscillation cycle match closely with those in the third quarter of the cycle and similarly the second matches with the fourth. This shows the dependence on whether the slip velocity is decreasing or increasing. Also in a typical sinusoidal curve the time instants of $0.1T$ and $0.9T$ would give the same exact value of x, hence giving the same value of slip length. But, we see that this is not the case here in the unsteady problem, thereby hinting the presence of hysteresis.

TABLE III. Fitting coefficients for collapsed data for various time instants over a time period. The time $t = 0$ corresponds to time of maximum slip velocity. This is done in order to remove the phase shifts between different runs. From the coefficients it can be seen that the first quarter coefficients match closely with the third quarter and similarly the second with the fourth.

t/T	a	b
0	0.64	1.0
0.1	0.46	1.22
0.2	0.14	1.23
0.25	0.02	1.32
0.3	0.03	1.77
0.4	0.43	1.22
0.5	0.64	1.15
0.6	0.47	1.22
0.7	0.15	1.22
0.75	0.01	1.37
0.8	0.04	1.6
0.9	0.44	1.2

F. Hysteresis

The lagging of fluid velocity due to fluid inertia suggests the presence of hysteresis and forms the motivation to explore it in unsteady oscillating flows. In Fig. 10(a) the slip velocity at the wall is plotted against the wall velocity, and in Fig. 10(b) the change in slip velocity is plotted against the fluid shear rate. Two different time periods of wall oscillation, 40τ and 200τ, are considered in each figure to study the effects of inertia on hysteresis. A hysteresis loop is formed in both the figures, and the area confined within the loop is seen to decrease with increasing time period.

The effect of inertia in developing hysteresis as seen in Fig. 10 is explained here. This could be described by visualizing fluid layers in the vicinity of the wall during the time when the wall is approaching an extreme location in the cycle and then changing direction. As the wall approaches the extreme point in the oscillation all the fluid atoms are moving in the same direction as the wall. But, when the wall
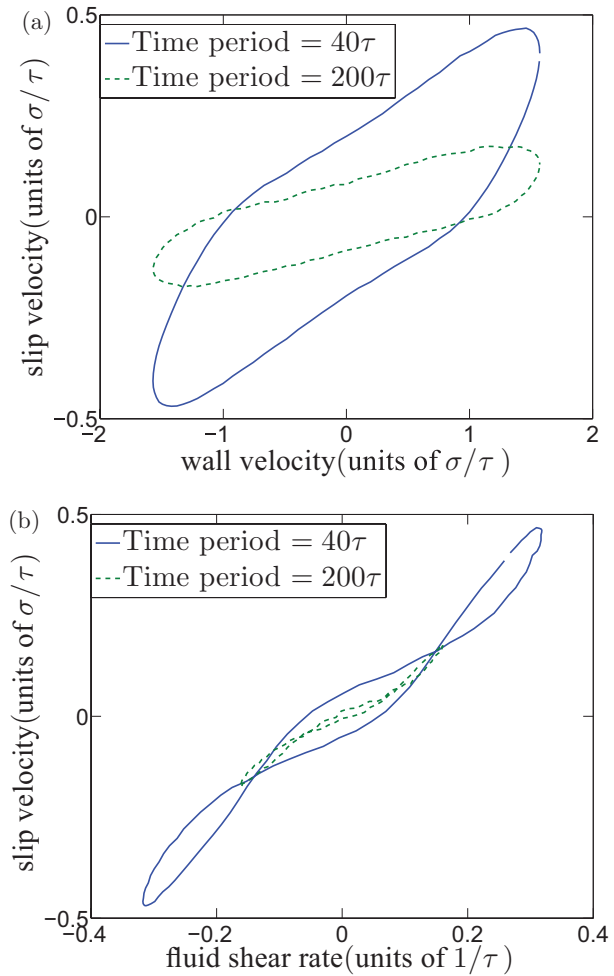
FIG. 10. (Color online) Slip velocity as a function of (a) wall velocity and (b) fluid shear rate exhibiting hysteresis is shown. The plots are for case 1 and amplitudes of 10σ and 50σ corresponding to time periods of 40τ and 200τ were chosen in order to maintain the same maximum wall velocity. All the curves are for a complete cycle of oscillations. It is seen that the area confined by the hysteresis loop decreases with increase in time period.

changes its direction the fluid adjacent to the wall does not change direction instantaneously as a result of inertia of fluid atoms in this and the neighboring layers. This leads to a change in the magnitude of fluid velocity, depending on the direction of motion of the wall, although they are evaluated at the same location of the wall in the cycle.

While there is a distinct loop observed in Fig. 10(a) at a time period of 200τ the loop in Fig. 10(b) collapses into a single curve. The area formed by slip velocity and wall velocity has the dimensions of energy per unit mass, while that formed by slip velocity and fluid shear rate has the dimensions of acceleration. Hence, the area in Fig. 10(a) could be possibly interpreted as the additional amount of energy the wall needs to transfer to the fluid below it in order to attain thermal equilibrium. This can be related to the lack of thermal equilibrium of fluid atoms adjacent to the wall which leads to slip. The area in Fig. 10(b) having the dimensions of acceleration can be correlated to inertia in the fluid. As the time period is increased from 40τ to 200τ we essentially reduce the inertia in the flow thereby getting closer to steady state which leads to the collapse of the loop.

The hysteresis here can be seen to be analogous to the commonly known magnetic hysteresis [44]. When a ferromagnetic material is subjected to magnetic field the atomic dipole aligns itself with the field but when the field is reduced to zero, partial alignment is retained. In order to demagnetize it a field must be applied in the opposite direction. This results in the difference in the path taken by the two legs in the hysteresis loop.

G. Energy dissipation in shear-driven flows

Understanding of the energy dissipation in shear-driven flows at small scales is important in designing some microsystem components, such as microcomb drive mechanism [30]. The dissipation may also lead to changes in fluid temperature which must be accounted for while performing experiments. The heat generation is a result of the viscous shearing of the fluid. As the temperature of fluid in the numerical experiments presented in this paper are maintained constant using a thermostat, the heat removed by the thermostat helps in determining the viscous heat generated by the system. In Fig. 11 the heat removed by the thermostat over time is plotted for steady and unsteady cases. The cases compared have identical wall-fluid properties and maximum velocity. It can be seen that the unsteady flow similar to that of the Stokes' second problem has a higher rate of energy dissipation than the steady Couette flow. This is due to the fact that the shear stress which is determined by the velocity gradient is higher for unsteady flow because of the presence of bounded Stokes' layers.

Our results from MD simulations performed on liquid argon reaffirm those presented by Karniadakis *et al.* [30]. They compare the shear stress and energy dissipation between simple Couette shear flow and oscillatory Couette flow for gases. They demonstrated that for flows beyond the quasisteady regime and for low Knudsen number values there is a significant increase in the magnitude of shear stress for oscillatory Couette flow as compared to simple Couette flow, consequently leading to increased energy dissipation. The increased energy dissipation in oscillatory shear flow has also been mentioned by Alsten
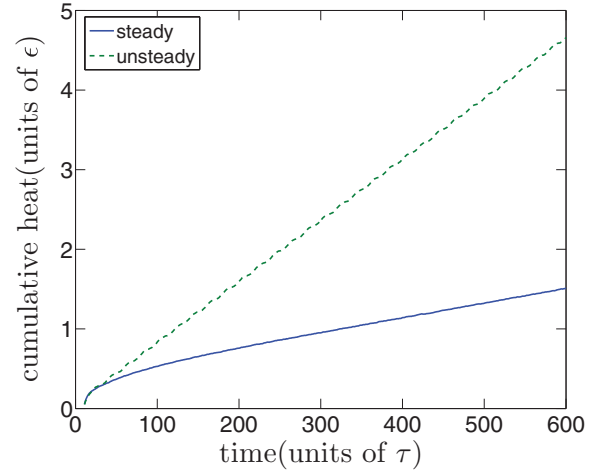
FIG. 11. (Color online) Cumulative heat removed by the thermostat versus time, for steady and unsteady cases with constant velocity amplitude of $1.57\sigma/\tau$. For the unsteady case the velocity is calculated for the wall displacement amplitude of 10σ and wall time period of 40τ. The wall-fluid properties used correspond to case 1. The rate of heat removed for the steady case is $0.002\epsilon/\tau$ and for the unsteady case is $0.008\epsilon/\tau$.

and Granick [34], who conducted experiments on ultrathin liquid film.

VII. CONCLUSION

A series of numerical experiments with different wall-fluid interaction properties and varying amplitudes and time periods were performed for a time-periodic oscillatory Couette flow problem. An increase in slip is observed as compared to the steady Couette flow problem. This increased slip was attributed to fluid inertial forces not represented in a steady flow. A case having wall-fluid properties that showed no slip for Thompson and Troian's steady Couette flow experiment is chosen. For this case when the fluid is subjected to an oscillatory flow a distinct slip is observed which confirms the increase in slip in an unsteady flow. To gain a deeper insight into the cause of the increased slip an unsteady slip model is established based on Maxwell's slip boundary condition. The dependence of slip on acceleration in addition to shear rate is shown. By writing acceleration in terms of shear rate, it is shown that slip at the wall depends on the gradient of shear rate and the shear rate of fluid at the wall. For the limiting case of steady flow the model reduces back to Maxwell's model. This provides a more accurate prediction of slip for unsteady flow problem rather than simply using the steady Navier's or Maxwell's slip model. Nondimensionalizing the model by scaling the problem by the wall velocity and the characteristic length of Stokes' second problem leads to the collapse of data onto a time dependent yet universal curve independent of wall-fluid properties. Thereby with the knowledge of shear rate of fluid and time instant in a cycle, slip length can be calculated using the universal curve without having to perform any computationally expensive MD simulations. A key nondimensional number, defined as the ratio of phase speed to speed of sound, helps in explaining and characterizing the transition of slip boundary condition from finite to perfect

slip is also identified from this nondimensionalization. Phase lag in fluid velocity relative to wall is observed. The lag increases with decreasing time period of wall oscillation and increasing hydrophobicity.

Hysteresis is observed while comparing slip velocity with wall velocity and shear rate. The cause for hysteresis can be attributed to the inertia of fluid. It is seen that the area formed by the loop decreases with increase in time period of wall oscillation. For the case of slip velocity versus the shear rate the loop collapses to a curve as the flow tends to a steady flow at an increased time period. In the case of slip velocity versus the wall velocity the area inside the hysteresis loop can be related to the loss of energy transfer from the wall to the fluid. For the loop formed by slip velocity and shear rate the area can be said to be equivalent to inertia of the flow. The rate of heat generated by viscous shear is compared for the unsteady Stokes' second problem and simple Couette flow and has been shown that it is higher for the unsteady flow as a result of higher shear stress in the flow.

ACKNOWLEDGMENTS

[1] S. Goldstein, *Modern Development in Fluid Dynamics* (Clarendon Press, Oxford, 1938), Vol. 2, pp. 676–680.

[2] S. Goldstein, Annu. Rev. Fluid Mech. **1**, 1 (1969).

[3] O. I. Vinogradova, Int. J. Min. Process **56**, 31 (1999).

[4] C. L. M. H. Navier, Royale des Sciences de l'Institut de France **1**, 414 (1823).

[5] J. C. Maxwell, *The Scientific Papers of James Clerk Maxwell* (Cambridge University Press, Cambridge, 1890), Vol. 2, p. 703.

[6] J. L. Barrat and L. Bocquet, Phys. Rev. Lett. **82**, 4671 (1999).

[7] C. Denniston and M. O. Robbins, Phys. Rev. Lett. **87**, 178302 (2001).

[8] J. Gao, W.D. Luedtke, and U. Landman, Tribol. Lett. **9**, 3 (2000).

[9] J. Koplik, J. R. Banavar, and J. F. Willemsen, Phys. Rev. Lett. **60**, 1282 (1988).

[10] J. Koplik, J. Banavar, and J. F. Willemsen, Phys. Fluids A **1**, 781 (1989).

[11] N. Priezjev and S. Troian, Phys. Rev. Lett. **92**, 018302 (2004).

[12] N.V. Priezjev, J. Chem. Phys. **127**, 144708 (2007).

[13] N. V. Priezjev, Phys. Rev. E **80**, 031608 (2009).

[14] P. A. Thompson and M. O. Robbins, Phys. Rev. A **41**, 6830 (1990).

[15] P. A. Thompson and S. M. Troian, Nature (London) **389**, 360 (1997).

[16] J. Baudry, E. Charalix, A. Tonck, and D. Mazuyer, Langmuir **17**, 5232 (2002).

[17] E. Bonaccurso, M. Kappal, and H. J. Butt, Phys. Rev. Lett. **88**, 076103 (2002).

[18] S. E. Campbell, G. Luengo, V. I. Srdanov, F. Wudl, and J. N. Israelachvili, Nature (London) **382**, 520 (1996).

[19] S. Granick, Y. Zhu, and H. J. Lee, Nature Mater. **2**, 221 (2003).

[20] O. A. Kiseleva, V. D. Sobolev, and N. V. Churaev, Colloid J. Russ. Acad. Sci. **61**, 263 (1999).

[21] D. C. Tretheway and C. D. Meinhart, Phys. Fluids **14**, L9 (2002).

[22] C. Neto, V. Craig, and D. Williams, Phys. Rev. Lett. **87**, 054504 (2001).

[23] Y. Zhu and S. Granick, Phys. Rev. Lett. **87**, 096105 (2001).

[24] A. R. A. Khaled and K. Vafai, Int. J. Non-Linear Mech. **39**, 795 (2004).

[25] M. T. Matthews and J. M. Hill, Microfluid. Nanofluid. **6**, 611 (2009).

[26] M. T. Matthews and J. M. Hill, Acta Mech. **191**, 195 (2007).

[27] C. Ng and C. Y. Wang, J. Fluid Eng. **133**, 014502 (2011).

[28] J. H. Park, P. Bahukudumbi, and A. Beskok, Phys. Fluids **16**, 317 (2004).

[29] G. H. Tang, X. J. Gu, R. W. Barber, D. R. Emerson, and Y. H. Zhang, Phys. Rev. E **78**, 026706 (2008).

[30] G. Karniadakis, A. Beskok, and N. Aluru, *Microflows and Nanoflows, Fundamentals and Simulation* (Springer, New York, 2005), Vol. 29.

[31] J. Thalakkottor and K. Mohseni, Bull. Am. Phys. Soc. **57**(17), pp. 337, M26.4 (2011).

[32] J. Thalakkottor and K. Mohseni, *42nd AIAA Fluid Dynamics Conference and Exhibit, 25–28 June, 2012* (AIAA, New Orleans, Louisiana, 2012), AIAA 2012-3158.

[33] P. Bahukudumbi, J. H. Park, and A. Beskok, Microscale Thermophys. Eng. **7**, 291 (2003).

[34] J. Van Alsten and S. Granick, Phys. Rev. Lett. **61**, 2570 (1988).

[35] S. Plimpton, J. Comput. Phys. **117**, 1 (1995).

[36] M. P. Allen and D. J. Tildesley, *Computer Simulation of Liquids* (Clarendon Press, Oxford, England, 1987).

[37] L. Verlet, Phys. Rev. **159**, 98 (1967).

[38] T. I. Gombosi, *Gaskinetic Theory* (Cambridge University Press, Cambridge, 1994).

[39] L. B. Loeb, *The Kinetic Theory of Gases* (McGraw-Hill, New York,1934).

[40] M. Balda, LMFsolve: Levenberg-Marquardt-Fletchers algoritm for nonlinear least squares problem, MathWorks, 2007.

[41] R. Fletcher, *Modified Marquardt Subroutine for Non-Linear Least Squares. No. AERE-R–6799*, Atomic Energy Research Establishment (Harwell, England, 1971).

[42] R. A. Harris and S. A. Rice, J. Chem. Phys. **33**, 1047 (1960).

[43] S. Granick, Science **253**, 1374 (1991).

[44] G. Bertotti, *Hysteresis in Magnetism: For Physicists, Materials Scientists, and Engineers* (Academic Press, New York, 1998).